Janus Particle Synthesis and Assembly

By *Shan Jiang, Qian Chen, Mukta Tripathy, Erik Luijten, Kenneth S. Schweizer,* and *Steve Granick**

Janus particles, colloid-sized particles with two regions of different surface chemical composition, possess energetic interactions that depend not only on their separation but also on their orientation. Research on Janus and colloidal particles that are chemically patchy in even more complicated fashion has opened a new chapter in the colloid research field. This article highlights recent progress in both experiment and theory regarding synthesis and self-assembly of Janus particles, and tentatively outlines some areas of future opportunity.

1. Introduction

Colloidal particles are fundamental to nature and technology. In terms of length scale, they bridge small molecules (Å), which can only be approached by modern tools of electron microscopy, and big objects (100 μm), which can be easily observed by the human eye. In terms of motion, they are pushed around by the random collisions from thermal movement of liquid molecules surrounding them (Brownian motion). In terms of chemical composition, they can incorporate both inorganic and organic species upon design. They can be bacterial or the components that form the eyes of an insect in the context of biology, and they are even present in the milk we drink. Studies on colloidal particles not only endow us with insight into nature, but also provide building blocks for new materials we desire.

A few years ago, P.-G. de Gennes raised the concept of "Janus particles" in his Nobel Prize address.[1] He borrowed the name "Janus" from the Roman God who has two faces looking into opposite directions to describe a special class of colloidal particles with different chemical makeups on their two hemispheres. For example, one side of the particle can be hydrophilic while the other side can be hydrophobic. What de Gennes had in mind was that these amphiphilic Janus particles might behave like surfactant molecules to adsorb at the water–air interface, forming a monolayer that de Gennes described as a "skin that can breathe," since small molecules would still be able to diffuse through the interstices between the Janus particles in the monolayer.

These ideas were largely ignored in subsequent years, the brunt of research in the field of colloids focusing instead on particles whose surface chemical makeup is homogeneous.[2] The development of chemical synthetic methods now provides access to particles with a wide range of sizes and materials. The development of scattering and imaging techniques enables detailed study of the structure and dynamics of different phases formed by colloidal particles. Furthermore, advances in computation power and algorithms have opened up opportunities to simulate colloid particles in the digital world. Some results from these studies reveal that the principles that guide the condensed-matter physics of small molecules, such as the sublimation and dislocation dynamics of crystals,[3,4] are similar to those governing colloidal systems. This aroused great interest in using colloidal particles as a model system to study the self-assembly and transport of atomic systems. However, applications of the concept of Janus particles have been proposed only sporadically.[5] What restrained de Gennes' idea from becoming true was the lack of proper synthetic methods to fabricate Janus particles.

This Progress Report first discusses recent progress in the development of synthetic methods to form Janus particles, emphasizing the ability to fabricate Janus particles in large quantities and with control of the geometry. Next, a zeroth-order theoretical framework is introduced within which the self-assembly of Janus particles can begin to be understood. Following this, the self-assembly of both dipolar and amphiphilic Janus particles is discussed. Finally, we end with a tentative discussion of possible future developments, conceptual and technological. This report highlights certain developments and opinions of the co-authors and is not intended to be a comprehensive review of the entire field.

2. Synthesis of Janus Particles

When it comes to the synthesis of Janus particles, two important issues need to be addressed. One is the ability to control the geometry of the Janus particles, i.e., the relative areas of their two sides. The other one is the ability to produce Janus particles in large quantities, which will be vital for technological applications. So far, various ways to synthesize Janus particles have been developed;[6–10] however, only a handful of them provide satisfactory solutions to both of these problems.

[*] Prof. S. Granick, S. Jiang, Q. Chen, M. Tripathy, Prof. E. Luijten, Prof. K. S. Schweizer
Frederick Seitz Materials Research Laboratory
University of Illinois
Urbana, IL 61801 (USA)
E-mail: sgranick@illinois.edu

Materials
Views

www.MaterialsViews.com

**ADVANCED
MATERIALS**

www.advmat.de

PROGRESS REPORT

Early methods to synthesize Janus particles employed planar solid substrates as the protecting surface. A monolayer of particles is formed on a solid substrate, the side of the particles facing the substrate being protected from chemical modification of the other side. Different approaches, such as sputtering,[11] stamp coating,[12–14] and Langmuir–Blodgett deposition,[15] have been applied to chemically modify the unprotected side of these monolayer surfaces. These approaches offer good control over the surface area that undergoes chemical modification, but only a few milligrams of particles are produced in one batch, because the approach relies on modification of a monolayer. Later, more methods were developed with the capability to synthesize particles in large quantity. One method entails adding a small amount of water to a particle-in-oil dispersion, causing silica particles to aggregate through capillary forces into clusters, whose exterior then is chemically modified.[16] This interesting approach can produce gram-sized quantities of chemically modified sample, albeit without much control over the surface geometry.

In particular, control over the relative portions of the two regions of amphiphilic Janus particles (the kind of surface chemical modification that de Gennes had in mind) that are rendered hydrophilic and hydrophobic, respectively, is analogous to controlling the well-known hydrophilic–lipophilic balance (HLB) of classical molecular-sized surfactants.[17] For Janus particles, we refer to the balance between hydrophilic and hydrophobic elements as the ''Janus balance''; a strict quantitative definition was reported elsewhere.[18] Since we expect the Janus balance to be an important parameter in determining the self-assembly of Janus particles and the ability for Janus particles to stabilize emulsions, it is an important consideration when evaluating synthetic methods.

Recently, we developed a versatile method to produce Janus particles based on particle-stabilized emulsions, so-called Pickering emulsions.[19] This method can synthesize Janus particles with controllable geometry in a wide range of sizes and can be scaled up to synthesize particles in gram-sized quantities.

A schematic representation of the method is summarized in Figure 1. At a liquid–liquid interface (here, an emulsion of molten wax and water), particles whose surface energy is between that of the two liquids will adsorb onto the interface, thereby lowering the total free energy.[20] In the case of our wax–water system, untreated hydrophilic fused silica particles adsorb to the oil-in-water emulsion interface at an elevated temperature where the wax is molten. After the particles have fully adsorbed, the temperature is lowered to solidify the wax phase and lock the particles in place. Subsequently, chemical modification is carried out at temperatures where the oil phase is solid, thus ensuring the modification of only those faces of the particle that are not buried in wax. The use of a solidified oil phase offers several advantages. First, it freezes the particles into fixed positions during the chemical modification step, avoiding the possibility that adsorbed particles might wobble or rotate at the liquid–liquid interface. Indeed, particle rotation at the liquid–air interface

Steve Granick (B.A. Princeton University, 1978; Ph.D. Chemistry, 1982, University of Wisconsin) is Founder Professor of Materials Science and Engineering, as well as Professor of Chemistry, Physics, and Chemical and Biomolecular Engineering, at the University of Illinois at Urbana-Champaign.

has been reported by others.[15] Second, the presence of a solid oil phase presents advantages at the stage of separation and purification of the particles. Third, when two stages of chemical modification are intended, this eliminates the need to find a liquid–liquid combination where the reactant is soluble in only one liquid.

In experiment, scanning electron microscopy (SEM) images reveal that most of the particles adsorb at the emulsion droplet surfaces,[19] whereas only few particles are found inside the wax droplet (as viewed after the wax droplet is broken). The excess of particles dispersed in water are filtered and rinsed away. The Janus geometry is confirmed by visualizing particles that contain fluorescent dye attached to one hemisphere.

The geometry of Janus particles can be well controlled using this method because it thermodynamically depends on the three-phase contact angle of particles at the emulsion interface. One way to tune the three-phase contact angle of particles is to add small amounts of surfactant molecules with opposite charge compared to particle surfaces during the emulsification.[21] As illustrated in Figure 2, adsorption of surfactants onto the particle
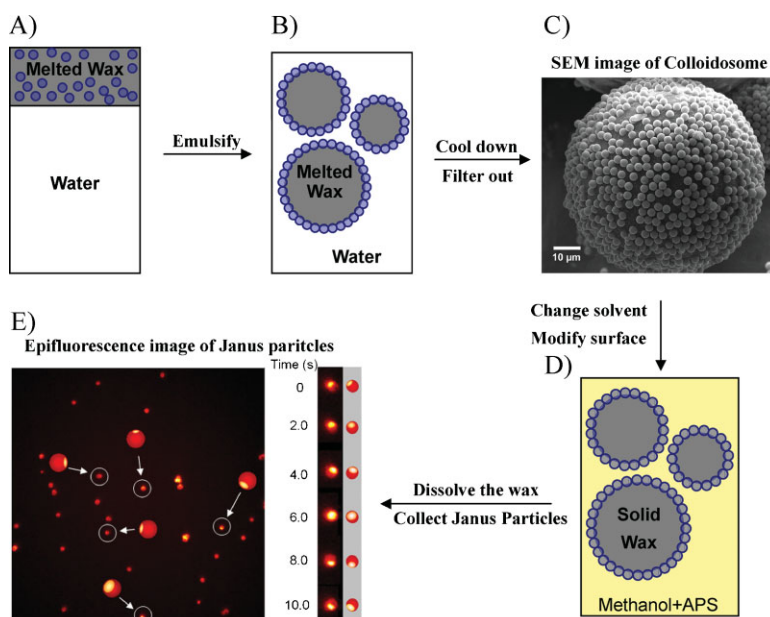

Figure 1. A–E) Schematic procedure to create Janus particles by functionalizing particles adsorbed onto an emulsion of water and oil and then cooling the sample so that the oil solidifies to form a wax. In a typical experiment, the wax-to-water volume ratio is 1:10, and particle loading is 2%. C) SEM image of a typical wax droplet (colloidosome). The size distribution of wax droplets is 20–150 μm. E) Fluorescence images of Janus particles with wax protected area labelled with fluorescent dye. On the right of the image the snapshots for one single particle at different times are shown. Adapted with permission from [19].
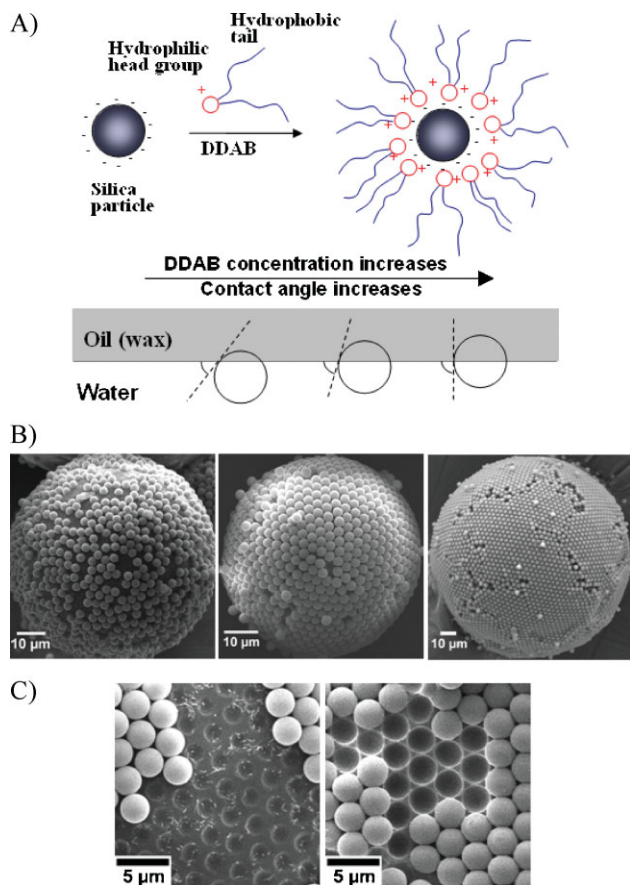
Figure 2. A) Schematic representation of the strategy used to control Janus geometry. Particles adsorb to the water–oil interface of emulsions, and the distance that the particle penetrates the respective phases determines a contact angle depicted by the dotted line. For silica particles, the cationic surfactant DDAB adsorbs strongly and renders the particle more hydrophobic, causing them to penetrate more deeply into the oil phase. Changing the surfactant concentration systematically varies the particle hydrophobicity, which results in systematic changes of the contact angle. Particles with different Janus balance can be obtained simply by controlling the amount of surfactant. The DDAB is rinsed off later using ethanol. B) SEM images of colloidosomes produced under different DDAB concentrations. From left to right the DDAB concentrations are 0, 20, 60 mg L^{-1} respectively. C) Contact angle was quantified from analysis of SEM images of voids left behind when particles are rinsed away from the wax surface by ethanol. From left to right, the colloidosomes were produced under DDAB concentrations of 20 and 60 mg·L^{-1} respectively. Adapted with permission from [21].

surface will render the hydrophilic particle surface more hydrophobic, thus causing particles to burrow more deeply into the wax phase and exposing a smaller area for further chemical modification. In this way, as more surfactants are added to the emulsion, particles embed deeper into the wax phase. After chemical modification, the surfactants facilitating the change of contact angle can be rinsed away by a simple solvent such as ethanol.

But how does one characterize the extent of surface chemical modification? One approach is to image the three-phase contact angle of particles at the emulsion interface by electron microscopy of the size of voids left by particles that escape from the wax surface during the processing steps. Such characterization yielded several interesting observations. It transpired that upon addition of surfactants to the emulsion the colloidal particles pack more closely and in a more ordered fashion on the wax surface as the surfactant concentration increases. It is estimated that more than 90% particles can be adsorbed to the emulsion surface depends on the surfactant concentration. The ordered packing is possibly due to screening of the electrostatic repulsion between like-charged particles at the interface, owing to the addition of surfactant molecules of opposite electric charge. The statistics analysis of contact angle revealed uniform distribution and similar variance for different surfactant concentration. The rationale behind this is that the contact angle is thermodynamically determined by the interfacial energy. It was also found that only surfactants of opposite electric charge could change the contact angle effectively; neutral surfactants or surfactants with the same charge as the particles failed to change contact angle over a wide range, since they do not adsorb strongly to the particle surface. The use of oppositely charged surfactants permits the chemical modification of particles as small as 100 nm in diameter.

To minimize the possible disruption of the wax droplet surface by mechanical stirring during the chemical modification step, a solvent-free modification method via vapor deposition of reactant molecules was developed to further improve the efficiency of this method.[22] Dry nitrogen or argon was bubbled through silane to bring silane vapor into contact with colloidosomes supported in a funnel. After investigations of several different types of silanes, those with low boiling point, such as dichlorodimethylsilane (DCDMS) and aminopropyldimethylethoxysilane (APS), were found to modify the silica particle surface most effectively under ambient conditions. Comparison of SEM images of untreated colloidosomes versus those of colloidosomes treated under solution-phase silane deposition and vapor-phase silane deposition demonstrated that the vapor-phase method resulted in much better adhesion of the silica particles to the wax droplet surface.

In summary, there are several advantages to the emulsion-based method to synthesize Janus particles. First, the reaction can easily be scaled up to synthesize large quantities of Janus particles, since large amounts of interfaces can be created during emulsification. Second, the Janus geometry can be thermodynamically controlled by the contact angle between the particle surface and the liquids used in the emulsion. Compared to alternative methods where the surface coverage of modified chemical makeup is controlled kinetically, this is easier to achieve, and the monodispersity of surface coverage is better from batch to batch. Also, a wide range of Janus geometries can be achieved by simply tuning the amount of surfactants added during the synthesis. Third, the chemistry that can be applied to this method is versatile. Besides the amphiphilic Janus particles mentioned here, also bipolar Janus particles, with opposite charges on each side, can be produced via this method.[22]

3. Theory

The formation of modulated phases, corresponding to a periodic density or concentration pattern in space, occurs in diverse

systems due to competing interactions, e.g., monolayers of molecules with short-range attractions and long-range anisotropic dipolar repulsions, oil-water-surfactant microemulsions, block copolymers, smectic liquid crystals, and ferrofluids.[23] The presence of competing attractions and repulsions leads to the possibility of either macrophase or microphase separation, and a Lifshitz point that defines the crossover from one inhomogeneous state of organization to the other. Block copolymer melts and solutions are perhaps the most studied member of this class of "frustrated" systems.[24] Here, local, monomer-scale enthalpic and/or entropic packing incompatibility in conjunction with chain connectivity constraints results in a rich order–disorder phase diagram. A Lifshitz point can occur in block copolymers in selective solvents of variable quality, or ternary polymer blend plus block copolymer microemulsions.[24] The disordered (and nearly incompressible) structure within a microdomain and relatively weak intermolecular interactions, along with the mesoscopic nature of the long-range order, allow successful mean-field theories to be constructed for the phase diagram (including the symmetries of ordered phases), based on a few simple ingredients such as an empirical Flory χ-parameter and incompressibility constraint.[25,26] On the other hand, self-assembly of compressible suspensions of Janus colloidal particles would appear to involve significantly different physics given their rigidity, strong and often short-range competing attractions and repulsions, and the hard packing constraints on a length scale commensurate with possible microphase ordering.

The competition between microphase and macrophase separation for homogeneous spherical colloids and nanoparticles that interact via spatially long-range and weak attractions and repulsions has been theoretically described based on a simple mean-field version of liquid-state theory.[27] This can describe the tendency of such particles to spatially order (a microphase spinodal or stability limit), though not the symmetry of the phase-separated regions. On the other hand, a prior microscopic theory of the structure and phase behavior of Janus colloids does not exist. Recently, two of us initiated the development of a theory using liquid-state physics methods that have been successfully employed for atomic, homogeneous colloidal, molecular and polymeric fluids. Our effort is inspired by the recent simulations[28] of cluster formation in dilute solution based on a model of a Janus particle as a collection of rigidly bound interaction sites on the surface of a sphere. Here we sketch the elements of the minimalist version of the approach and focus solely on determining macrophase and microphase separation at the level of a mean-field spinodal.

3.1 Theoretical Model of Janus Particles

We summarize the elements of the integral-equation theory in the context of a three-site model of a Janus particle: small A and B interaction sites of diameter d that cover the surface of a hard spherical core (site C) of diameter D. The starting point is the Reference Interaction Site Model (RISM) theory of Chandler and Andersen,[29] which can predict the statistical pair structure, thermodynamics, scattering structure factors, and macroscopic phase behavior of fluids of rigid molecules. Over the past two

decades, this approach has been extensively generalized and applied to flexible macromolecular and hybrid organic–inorganic mixture systems, including polymer solutions and melts, blends and block copolymers,[30] polymer–particle suspensions and nanocomposites,[31] and nanoparticles that carry grafted tethered chains dissolved in concentrated solutions or homopolymer melts.[32,33] The molecular species are represented as a collection of bonded sites that interact via pair decomposable site–site potentials that include a hard-core excluded-volume repulsion which defines their size, and chemically-specific non-contact site–site pair potentials, $U_{ij}(r)$, e.g., van der Waals, hydrophobic or Coulomb interactions. The theory is defined by a set of coupled nonlinear matrix integral equations:[29,30]

$$\underset{\sim}{H}(r) = \int d\vec{r}' \int d\vec{r}'' \, \underset{\sim}{\Omega}(|\vec{r} - \vec{r}'|) \underset{\sim}{C}(|\vec{r}' - \vec{r}''|) \underset{\sim}{\Omega}(r'')$$
$$+ \int d\vec{r}' \int d\vec{r}'' \underset{\sim}{\Omega}(|\vec{r} - \vec{r}'|) \underset{\sim}{C}(|\vec{r}' - \vec{r}''|) \underset{\sim}{H}(r'') \qquad (1)$$

Here, $\underset{\sim}{H}(r)$ contains elements $\rho_i \rho_j h_{ij}(r)$, where $h_{ij}(r) = g_{ij}(r) - 1$ is the nonrandom part of the intermolecular pair correlation or radial distribution function between sites of type i and j, ρ_k is the site number density of species k, $\underset{\sim}{C}(r)$ contains elements $C_{ij}(r)$ which are renormalized site–site intermolecular potentials or "direct correlation" functions, and $\underset{\sim}{\Omega}(r)$ is a matrix that defines the intramolecular pair correlations which is linear in site number densities and for rigid Janus colloids can be determined from elementary geometry. To render the number of integral equations tractable, geometric (not chemical) site inequivalency is pre-averaged as done for polymeric systems.[30–33] Hence, for a Janus particle, Equation 1 is a 3×3 matrix that describes six distinct site–site pair correlation functions: $g_{aa}, g_{ab}, g_{bb}, g_{ac}, g_{bc}, g_{cc}$.

Equation 1 requires an approximate closure which provides a second set of relations between the correlation functions and potentials. Reliable closures for systems with large structural asymmetries and/or strong and short-range interparticle interactions are not obvious. In this initial work the simplest random phase approximation (RPA) description, extensively employed in polymer field theory,[25,26] is adopted for all correlations except the core–core correlations. This corresponds to:

$$C_{ij}(r) = C_{ij}^{(0)}(r) + \Delta C_{ij}(r) \qquad (2)$$

where an "athermal reference" system is introduced defined as when $U_{ij} = 0$ with $g_{ij} = 0$ inside the distance of closest approach. Numerical solution of the RISM equations for this reference system determines $C_{ij}^{(0)}(r)$. The effect of non-contact potentials is given by:

$$\Delta C_{ij}(r) \approx -\beta U_{ij}(r) \qquad (3)$$

where β is the inverse thermal energy. The hypernetted chain closure is adopted for the purely excluded-volume core–core direct correlations:

$$C_{cc}^{(0)}(r) = h_{cc}^{(0)}(r) - \ln g_{cc}^{(0)}(r) \qquad (3a)$$

$$\Delta C_{cc}(r) = 0 \qquad (3b)$$

Equations 1–3 yield the pair correlation functions. The collective partial scattering structure factors in Fourier space, $S_{ij}(k)$, that describe correlated concentration fluctuations over all length scales, follow as

$$\underline{S}'(k) = \underline{\Omega}(k) + \underline{H}(k) = (\underline{I} - \underline{\Omega}(k)\underline{C}(k))^{-1}\underline{\Omega}(k) \qquad (4)$$

where I is the identity matrix, and $S'_{ii} = \rho_i S_{ii}$. As $k \to 0$, the $S_{ij}(k)$ quantify bulk partial number density fluctuations, and their divergence signals macroscopic spinodal phase separation. Microphase separation corresponds to the divergence of all structure factors at a nonzero wavevector, k^*, the inverse of which defines the spatial periodicity. The length scale of spatial ordering (L^*) is related to the divergent wavevector as $L^* = 2\pi/k^*$. Note that in RISM theory the intermolecular structure is functionally related to the intramolecular structure and to bare interparticle interactions, and excluded volume is rigorously enforced (here just in the athermal reference fluid). This RISM-RPA approach has been previously employed for microphase separation in block copolymers[30] and mixtures of nanoparticles with grafted chains in a homopolymer matrix,[32,33] and macrophase separation in polymer blends.[30] Use of Equation 2 allows a nearly analytic and rapid computation of spinodal phase diagrams once the athermal reference system correlations have been numerically obtained.

3.2 Theoretical Calculations of the Phase Diagram

Calculations have been performed for Janus particles composed of 72 elementary surface sites of diameter equal to 20% of the core diameter ($d = 0.2D$), which interact via non-contact potentials. The composition or Janus balance is 50/50. The model is illustrated in Figure 3c. The B sites attract via a square well potential of range $0.1D$ and contact strength $-\varepsilon_b < 0$, and the A sites repel via a square-well potential of range $0.1D$ and strength ε_a; the A–B cross interaction is purely hard-core. Temperature is reported in units of $-\varepsilon_b$, and the non-contact repulsion strength via the ratio $|\varepsilon_a/\varepsilon_b|$. The spatial ranges are chosen to mimic the model employed in the Janus particle simulation study,[28] when A is charged and B experiences a hydrophobic attraction.

Figure 3a presents the phase diagram in the representation of reduced temperature versus particle volume fraction. The corresponding unstable or ordering wavevector, k^*, is shown in Figure 3b. There are multiple interesting features in these two figures. Consider first the uncharged system ($\varepsilon_a = 0$). At low volume fractions, the unstable wavevector occurs at $k^* = 0$, corresponding to macrophase separation into Janus-particle rich and Janus-particle poor coexisting phases. This is analogous to a liquid–vapor type demixing transition. However, beyond $\phi = 0.05$ there is a crossover (Lifshitz point[23,27]) to microphase separation corresponding to ordering on a finite length scale (nonzero k^*). As the volume fraction further increases, the microphase separation temperature and ordering wavevector both increase. The transition temperature becomes roughly constant for $\phi \sim 0.2$–0.35, and then further increases at high volume fractions; the ordering wavevector nearly saturates at a value corresponding
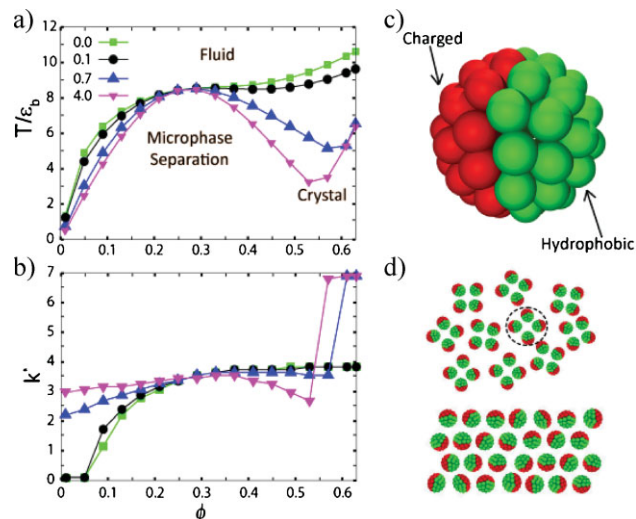

Figure 3. a) Spinodal phase diagram for the four indicated ratios of the absolute magnitude of the repulsive (ε_a) to attractive (ε_b) non-contact interaction. b) The unstable or ordering wavevector (k^*) for the four systems analyzed in (a). The results show that crossover (Lifshitz point) from a macrophase to microphase separation boundary occurs for the two weaker repelling Janus colloids at a system-specific volume fraction. In contrast, the two strongest repelling Janus particle systems always undergo an ordering transition at nonzero k^*, of either microphase or simple crystallization character. c) A schematic of the model of the Janus particle adopted for the RISM calculation. d) Speculative qualitative real-space organizations in the microphase-separated state are shown corresponding to when $k^* \sim 3$, for intermediate volume fractions (top image) and highest volume fraction crystalline state (bottom image).

to a real space periodicity of $2\pi/k^* \sim 2D$. An educated guess of a possible real-space structure is indicated on the right side of Figure 3d.

As the non-contact repulsion between A sites is turned on, the phase diagram and ordering wavevector first undergo quantitative, and then qualitative, changes. For a weak repulsion of $|\varepsilon_a/\varepsilon_b| = 0.1$, the phase boundary shape is qualitatively the same, and k^* nearly identical, as when $\varepsilon_a = 0$. When $|\varepsilon_a/\varepsilon_b|$ grows to 0.7 and then 4, a maximum emerges in the phase boundary at $\phi \sim 0.28$, followed by a minimum. The latter indicates suppression of microphase ordering with increasing particle concentration. We speculate that this may be due to the formation of clusters or aggregates, which at modestly high volume fractions experience a degree of packing frustration that makes it more difficult to form a periodic microphase. At even higher volume fractions the transition temperature again rises and a regime is entered that is reminiscent of hard-sphere colloid crystallization. This interpretation is supported by the discontinuous jump of k^* at high volume fractions to a value corresponding to a spatial periodicity of one Janus sphere diameter, i.e., a close-packed crystal. A speculative cartoon of the possible real space structure in this ultra-dense regime is shown in Figure 3d.

Note also that increasing the repulsion between A hemispheres always results in a (modest) reduction of the phase transition temperature, except at a "pinch point" where all phase boundaries appear to intersect at $\phi \sim 0.28$. The shape of the phase diagram for $|\varepsilon_a/\varepsilon_b| = 4$ system is reminiscent of a simple

Materials
Views
www.MaterialsViews.com

ADVANCED
MATERIALS
www.advmat.de

PROGRESS REPORT

liquid such as argon that has a liquid–vapor critical point and a liquid–crystal transition. However, this analogy does not apply to the present Janus particles. The reason can be seen in Fig. 3b, which shows that for $|\varepsilon_a/\varepsilon_b| = 0.7$ (and larger) all macrophase separation transitions are destroyed due to the frustration associated with the extra repulsion, and are replaced by a microphase transition for volume fractions up to ∼0.52–0.56, and then a simple crystallization-type transition at the highest concentrations.

3.3. Outlook

The liquid-state theory described here rigorously captures, in the athermal limit, the excluded-volume packing constraints of spheres composed of elementary surface sites. However, it adopts a minimalist, simple analytic mean-field description (RPA) of the consequences of non-contact attractive and repulsive interactions between Janus particles. As has been done in the most advanced liquid-state theories of block copolymers,[30] polymer nanocomposites,[31,34] and tethered nanoparticles,[32,33] it is important to go beyond this RPA description to include fluctuations effects which can significantly modify the microphase order–disorder transition.[24,25] Efforts in this direction are underway. In the longer term, the development of predictive density-functional theories[35] to describe the symmetries of the ordered microphases is desired. This task likely will require knowledge of all the homogeneous phase correlation functions as input to the free-energy computation. The role of metastable liquid–liquid demixing boundaries on microphase separation is also important to understand and control, as vividly demonstrated for crystal nucleation in nanoparticle, colloid and protein suspensions.[36] Moreover, the tendency of sticky and/or high volume-fraction particle suspensions to become trapped in nonequilibrium states (gels, glasses) requires the development of new microscopic dynamical theories. Kinetic gelation or vitrification can be undesirable since it frustrates ordered self-assembly. On the other hand, dense and soft amorphous solids are generally desirable as inks for direct-write printing materials engineering applications.[37] For all the above issues, large-scale computer simulations of Janus particle fluids far beyond the dilute regime are essential to provide benchmarks tests of the inevitable statistical-mechanical approximations.

4. Self-Assembly

In nature and technology, many useful structures arise through self-assembly, e.g., protein folding and self-assembled monolayers (SAMs). In the field of colloid research, experiments now appear poised to implement the vision of "molecular colloids" whose patchy surface chemical makeup governs their assembly into super-structures.[38] Indeed, the assembly of larger (non-Brownian) objects has already been implemented.[39,40] On the other hand, most of the "useful" structures self-assembled from patchy colloidal particles only exist in simulations, such as crystal structures with diamond symmetry and "lock-and-key" structures.[41] Experimental evidence that these structures can

actually be self-assembled by colloidal particles is scarce. Here we study the self-assembly or cluster formation of Janus particles under dilute concentration conditions in both experiment and simulation. Due to the difference in nature of their interactions, the self-assembly of dipolar Janus particles[42] and amphiphilic Janus particles[28] are completely different and will be discussed separately.

4.1. Self-Assembly of Janus Dipolar Particles

A dipolar Janus particle, with opposite electric charge on its two hemispheres, is the colloidal analogue of a dipole. In this particular experiment, Janus particles were synthesized by directional coating. First, a monolayer of particles was deposited on a flat substrate. Then a thin adhesion layer of Ti (2 nm) and a thin layer of Au (15 nm) were deposited on the upward-facing side of the particles. The Au-coated surface was further rendered positive using thiols with positively charged amine groups. The other hemisphere was negatively charged with carboxylic acid groups on the untreated side of carboxylate-modified polystyrene colloids. From measurement of the zeta potential of Janus particles,[43] the net particle charge was estimated to be nearly zero. The experiments were conducted in PBS buffer (pH = 6) at 1 mM ionic strength, such that the Debye screening length was approximately 10 nm.

To model these dipolar Janus particles, spherical shells were composed of much smaller, isotropically distributed spherical particles.[43] The large number of surface particles ensures a smooth representation of the charge distribution on each hemisphere. The interaction between two Janus particles was modeled by assigning an attractive or repulsive square potential between each pair of surface particles according to the sign of both hemispheres, and the range and magnitude of the interaction were tuned to represent their screened electrostatic interaction. The results are insensitive to the precise range (and shape) of the particle potential (and hence to precise salt concentration), as long as this range is less than 30% of the colloid diameter.

As described in more detail elsewhere,[42] in the simulations we first obtained the colloid pair potential by systematically exploring all possible relative orientations of a pair of Janus particles. Then this pair potential was fitted to a functional form. We explicitly verified that variation of the number of surface particles does not change the shape of this potential, but merely rescales the contact energy of a pair of Janus particles. The magnitude of the colloid potential quickly decays to zero with increasing surface-to-surface distance. Subsequently, we carried out Monte Carlo simulations in which the Janus particles were represented as monodisperse hard spheres with a pairwise interaction given by the functional form obtained. Use of this functional form allowed us to study systems containing relatively large numbers of particles for a large number of steps, which is essential to ensure that stable configurations are reached. The simulations employed a standard Monte Carlo algorithm and were all performed in the *NVT* ensemble with periodic boundary conditions.

In order to conceptually analyze the interactions between dipolar particles, it is useful to consider a polar axis pointing north–south through the hemispheres. Only if the axes of the two
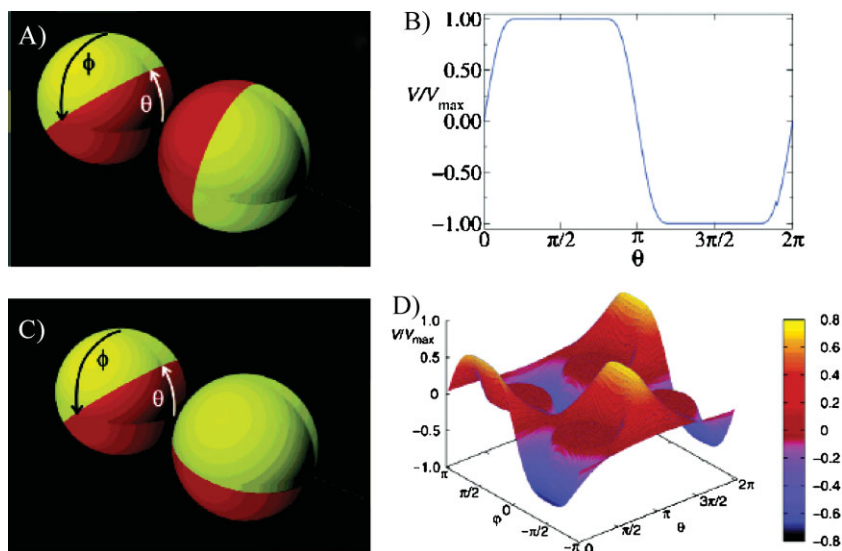
Figure 4. Interaction potential between two particles with bipolar charge. The right object is fixed; the angles (θ, φ) indicate the orientation of the left object. Red denotes positive charge, and yellow denotes negative charge; these charges are equal in magnitude. A) Charged hemispheres whose polar axes lie in the same plane. B) Relative interaction energy for case A, plotted against angular displacement for two particles at contact. The interaction potential switches from repulsive to attractive as the left-hand object rotates in the θ direction even when the particle–particle separation does not change. C) General case where the polar axes do not lie in the same plane. D) For every orientation of the right-hand particle, a potential energy landscape must be determined. Thus, the parameter space becomes four-dimensional even at fixed surface separation, illustrating the rapid increase in complexity once one goes beyond the concept of isotropic potentials. Reproduced with permission from [43].

Janus particles lie in the same plane (Fig. 4A), the interaction changes smoothly from repulsive to attractive depending on how the particles face one another. As illustrated in Figure 4B, this switch occurs over a narrow range of rotation angle. Generally, the polar axes passing through the hemispheres do not lie in the same plane (Fig. 4C), and the interaction potential depends on relative orientation as well as on separation. This multidimensional parameter space illustrates the rapid increase of complexity as one goes beyond the classical concept of isotropic potentials. Figure 4D presents the calculated dependence of the interaction potential on the two polar angles describing the orientation of one particle for a fixed orientation of the second particle and for fixed particle separation.

A key conclusion of Figure 4 is the existence of multiple energetic minima. Experiments confirmed this expectation. Epifluorescence images show that particles always cluster into specific geometrical shapes depending on the number of particles, as summarized in column A of Figure 5, and Monte Carlo computer simulations (column B of Figure 5) agree well with these experiments. Since the orientation of individual particles cannot be resolved by experiment, we further exploited the modeling to determine the mutual orientation of the charged hemispheres on neighboring particles. For the case of $N = 2$ particles, one observes that the particles find a low-energy state even if their polar axes do not lie strictly in the same plane. This broad energy minimum is expected, since the area of contact is much smaller than the particle size. For clusters larger than $N = 2$, the polar axes of the hemispheres twist in space as neighboring particles circle the structure.

As we discuss elsewhere,[42] one profound consequence is that the envelope of electrostatic charge is not distributed evenly if one considers the entire cluster as a particle in its own right. In another word, the clusters formed by dipolar particles are also dipolar as a bigger object. To illustrate this, Column C of Figure 5 displays the envelope of electrostatic charge presented by each cluster to its environment (the caption of Figure 5 describes the color coding). Charge is distributed asymmetrically; one half of each (non-spherical) cluster tends to be predominantly positive in charge, the other half predominantly negative, so that the charge asymmetry on the elemental spherical particles is preserved in the surface charge asymmetry of the clusters into which they assemble.

In principle, there appears to be no limit to the size of clusters that can form from these electrostatic interactions; our modeling shows that each cluster of larger size is energetically more stable than all of the smaller ones. This implies that if only the concentration were higher, the positive side of one cluster would attract the negative side of another cluster, resulting in facile assembly into even larger aggregates.

The compact cluster shapes in Figure 5 differ fundamentally from the widely studied lines and rings formed by magnetic particles[44] and electric dipoles.[45] Our particles would behave as ideal dipoles only at distances that much exceed the actual interaction range.

Another interesting comparison is to the "clusters" formed by homogeneous particles,[46] whose structures are those predicted mathematically for optimally dense packing. For $N = 2$–5 and $N = 7$, we observe that dipolar Janus particles assemble into clusters with the same overall shapes, albeit with the internal structure and charge asymmetry depicted in Figure 5. By contrast, for $N = 6$, 11, 12, and 13, the shapes found for hemispherical interactions differ from those obtained from isotropic interactions. The difference is that the shapes we observe are less symmetric. We anticipate even larger distinctions for particles of lesser symmetry, for example, unmatched positive and negative surface charge, and also for larger clusters, but this aspect remains open for future detailed elucidation.

Another key aspect of these Janus particles is that real-time imaging reveals the kinetic process of self-assembly. The constituent zwitterionic spheres assemble into clusters, then the clusters coalesce with one another, and structural defects heal, all of this is on the time scale of seconds to minutes. In most of the earlier work on colloid clusters, the conditions were such that in the ultimate structures the elements were quenched in place.[46] In the present system, interactions are relatively weak. From the simulations we estimate them on the order of 5–10 $k_B T$ and this is consistent with the unambiguous observation of equilibration events—dynamical particle attachment to and detachment from clusters, and reconfiguration of cluster
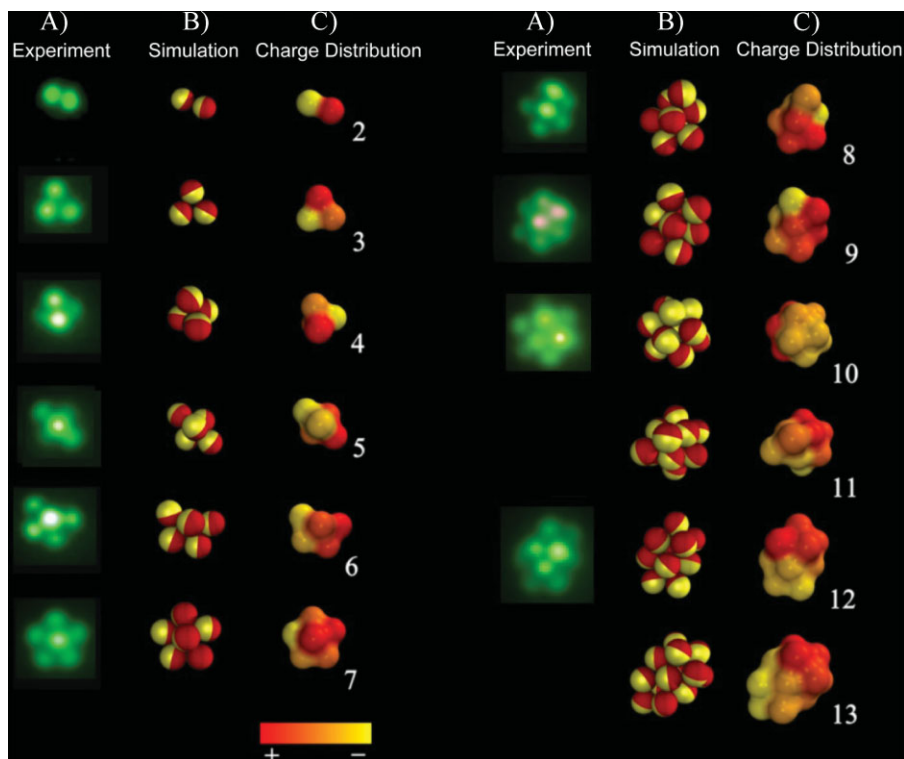
Figure 5. Comparison of experimental epifluorescence images and Monte Carlo computer simulations of the self-assembled structures of particles with near-equal positive and negative charges on the two hemispheres (denoted by red and yellow colors). Clusters form with monotonically decreasing energy as the number of colloidal particles increases. Their computed structures (column B) agree quantitatively with the observed structures (column A). The charge distribution in these clusters is also computed; the color goes smoothly from red to yellow depending on the inner product of the vector from the center of mass of the cluster to each colloid and the axial vector (pointing to the positive side) of this colloid (column C). In the charge distributions, a wrapping has been added to emphasize the outer surface. As described in the text, experimental measurements of zeta potential showed it to be <1 mV, confirming that the charge on the two hemispheres was nearly balanced. Reproduced with permission from [43].

shapes—in video images. This experimental approach will allow comparison with prior computer-based calculations of how patchy particles associate.[45,47–51]

It is straightforward to apply the same modeling approach to colloids whose shape is not spherical, such as rodlike or oblate particles. The bipolar functionality studies can also be generalized to ternary or even more complicated patchy geometries: a simple place to start would be to divide spheres into three regions of different chemical composition, as appears to be possible by vacuum deposition of metal at oblique angles. Finally, it is intriguing to note that asymmetric charge distribution has been proposed, based on experiments, to explain the aggregation of some proteins.[52] Thus, these model particle systems may have some relevance to proteins and other more complex particles where the surface charge distribution is similarly patchy.

4.2 Self-Assembly of Janus Amphiphilic Particles

The second case of Janus particles we discuss are amphiphilic particles, hydrophobic on one face and charged on the other. Although the interactions between these particles have an anisotropy that is similar to that found for the dipolar particles

considered in the previous section, the resulting aggregates have structures that differ greatly from those presented in Figure 5. In water, the interactions can range from an extreme of hydrophobic attraction when the hydrophobic sides face each other to a limit of electrostatic repulsion when two charged sides face one another, as shown in Figure 6. This orientation-dependent interaction organizes Janus particles into aggregates rich both in terms of dynamic pathways and final shapes compared with particles of homogeneous chemical makeup. Since only the hydrophobic hemispheres attract, the system is simpler than the dipolar particles considered above.

On the experimental side, the low density of latex particles reduces the propensity to sediment and allows one to investigate more systematically three-dimensional self-assembly. As discussed in Reference [28], amphiphilic parent particles are created by spreading them onto a clean glass slide and coating them with a thin film of gold. Conventional thiol chemistry with octadecanethiol is applied onto the gold film to form a self-assembled monolayer and render the gold covered hemisphere hydrophobic. After rinsing away the residue chemicals, particles are dispersed in water by ultrasonication and observed under an epifluorescence microscope. The particles used are 1 μm in diameter, which enables the resolution of individual particles under the microscope and also the observation of compact three-dimensional structures within the depth of view. The volume fraction is small, around 10^{-3}.
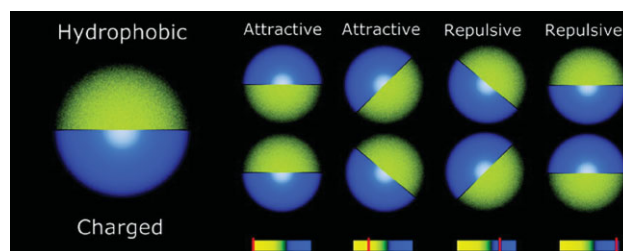

Figure 6. Pairs of colloidal particles in water, each hydrophobic on one hemisphere and charged on the other (denoted by yellow and blue colors), are considered at fixed separation. The interaction potential switches from attractive when the hydrophobic sides face one another (left) to repulsive when the charged sides face one another (right), with intermediate attraction or repulsion at canted angles (middle). Below each particle pair, the intensity of the interaction potential at that mutual orientation is shown schematically. Reproduced with permission from [28].

The experiments are analyzed via Monte Carlo simulations.[28] The orientation-dependent interaction potential consists of three terms: an isotropic repulsive hard core to prevent particle overlap, a hydrophobic attraction between the hydrophobic hemispheres, and an electrostatic repulsion between the polar sides of the particles; both the hydrophobic attraction and electrostatic repulsion are modulated further according to particle orientation regarding their Janus character. In particular, electrostatic repulsion is described by a pairwise Debye–Hückel potential, within which the salt concentration plays a role by changing the ionic strength. In treating the hydrophobic interaction, a minimalistic model is used to avoid the controversial question of the mechanism of hydrophobic attraction, which is not the problem at hand.[53] Instead, a simpler route is taken based upon the conclusion extracted from the available experiments that the attractive hydrophobic interaction is short-ranged compared to the particle diameter, decaying roughly exponentially with interparticle separation with a decay constant on the order of 10 nm under normal circumstances. In addition, it is barely affected by suspension salt concentration. Accordingly, an attractive square-well potential with a range of 5% of the particle diameter is chosen to represent the hydrophobic attraction in this particular system. The computer simulations employ a standard Monte Carlo algorithm for thousands of particles and are all performed in the NVT ensemble with periodic boundary conditions. The final structures are reached after around 10^6 sweeps for all runs, adequate to ensure equilibration of the system, as described elsewhere.[28]

The observed self-assembled structures of amphiphilic Janus particles show a strong dependence on salt concentration, as seen in Figure 7. First, in deionized water, the amphiphilic spheres repel one another so strongly that they remain individual. However, when the electrostatic screening length falls to 10 nm at higher salt concentration, clusters form with the property that, for each number (N) of spheres in the cluster, the cluster possesses a definite, compact configuration. When the electrostatic screening length is further reduced by a factor 2.2 by adding more salt, the smaller clusters polymerize into extended, branched, wormlike objects. Besides direct imaging of final structures, the fluorescence microscopy experiments are unambiguous in revealing equilibration events on time scales of seconds to minutes as these clusters self-assemble. For example, two distinct configurations are observed for the tetramer shape, $N = 4$. One of these is the conventional tetrahedron and the other is less densely packed, and they are observed to interconvert dynamically. These structures and their dynamics match with predictions made from the corresponding Monte Carlo simulations, which indicates that the system is equilibrated and driven by minimization of free energy. Owing to the relatively weak particle–particle interactions it is easy for the particles to escape from the attraction and rearrange, and the clusters possess no definite, frozen shape; instead, they wriggle and change their configurations with time.

The other significance of the agreement between experiments and simulation is the validity to use time sequences in simulation to suggest the actual mechanism of worm-like chain growth. Although the Monte Carlo simulations do not reproduce the actual dynamics of the Janus particles, the exclusive use of local particle moves makes it possible to attach a dynamic
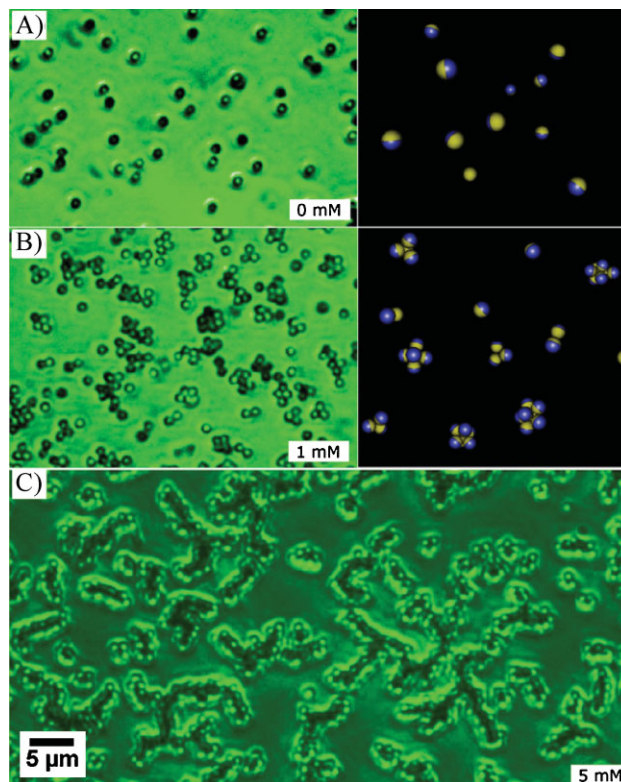

Figure 7. Varying the salt concentration causes amphiphilic particles (1 micron diameter) to assemble into clusters of various sizes and shapes. The images with green background represent epifluorescence experiments. In the computer simulations, blue and yellow colors represent charged and hydrophobic hemispheres, respectively. Panel (A) shows discrete particles are present in deionized water. Panel (B) (1 mM KNO$_3$) shows small clusters (up to nonamers) in equilibrium with one another. Panel (C) (5 mM KNO$_3$) shows long, branched wormlike strings. The simulations (right) confirm that the assembly of small clusters into strings occurs as the range of the electrostatic repulsion, relative to hydrophobic attraction, decreases with increasing salt. Reproduced with permission from [28].

interpretation to the simulation results. In particular, a heptamer, as one of the most stable clusters whose detailed shape nonetheless breathes dynamically, is a crucial building block of the chain. Successive simulation snapshots show the formation of a heptamer from the fusion of a trimer and a tetramer. Later, during the fusion of a heptamer with another cluster, the former imprints its topology upon the latter, leading to the linking of clusters into a worm-like chain. Geometric frustration arising from simultaneously satisfying the hydrophobic attractions and the electrostatic repulsions causes the string to rearrange and bend. Based upon this detailed analysis, a lock-and-key mechanism is proposed, in which wormlike strings are formed by the polymerization of clusters instead of through sequential addition of individual particles. This gives insight into the formation mechanism of chains observed in experiments.

5. Applications – Scientific and Technological

Now it is appropriate to pose the question of how to use Janus particles – to what purpose might they be applied?

5.1 Self-Assembly

The structures formed by Janus amphiphilic particles as described in Section 4.2 are analogous to the micellar shapes adopted by standard molecular amphiphiles. This similarity can provide an approximate idea of the fundamental rules followed by even more complex molecular systems such as the phase behavior of diblock copolymers and functionality of biological membranes assembled by phospholipids. A more detailed understanding of these systems would be built upon the answers to several more delicate questions. A comprehensive study of the phase behavior of the amphiphilic Janus particles, how they evolve from dilute solution to concentrated suspensions, might go beyond the conventional phase diagram for homogeneous colloids by revealing new behavior such as microphase separation. Inspired by the assembly behavior of surfactants, we also expect that the self-assembled structures of amphiphilic Janus particles depend on—and can even be controlled by—the Janus balance, the relative surface areas of the hydrophobic and charged patches. Eventually the question that needs to be answered is what new assembled structures can form when Janus amphiphilic particles of different size, surface chemistry and possibly Janus balance are mixed together, since real systems typically contain more than one component. On the application side, amphiphilic Janus particles can serve as solid surfactants that adhere to the oil–water interface, thereby stabilizing emulsions and foams. Moreover, the wormlike strings, or even the clusters, may also modify suspension rheology to produce different glass or gel dynamics and yielding behaviors, and they may be used as environment-responsive vehicles within which to encapsulate cargo for subsequent controlled release. The idea of having solid surfactants generalizes the concept of molecular amphiphilicity that is so pervasive and useful in nature and technology.

5.2. Janus Particles as Optical Probes for Microrheology

Going beyond questions of self-assembly, transport problems are also worth emphasizing. Janus particles can display anisotropic transport under certain conditions. This is usually due to the different local flow profiles or osmotic potential induced by the external field or chemical reactions. It was found that Au-coated Janus particles will diffuse perpendicular to the external electric field,[54] due to the induced-charge electrophoresis flow close to the particle surface of different hemispheres. The effective net force pushes particles to move in the direction perpendicular to the external electric field. Another way to move Janus particles in a certain direction is by self-propulsion induced by a catalytically active surface.[55] This may find its application in drug delivery systems, since self-motile particles can move more efficiently than conventional Brownian particles.

Another potential utilization of Janus particles is to use them as tracers to probe the local rheological properties of their environment. The contribution here is to use modulated optical nanoprobes (MOONs) whose optical properties are modulated by their rotational diffusion, thus augmenting the information about position that is obtained from conventional translational
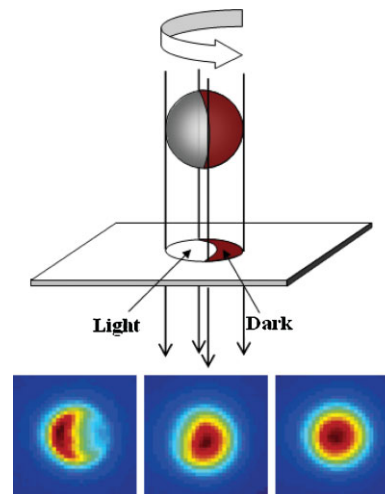

Figure 8. The idea of measuring rotational diffusion using MOON particles, fluorescent on one side and "dark" on the other, is illustrated. a) Schematic illustration of this idea. b–d) Images of a MOON particle, 2 μm diameter, for three orientations ranging from crescent to full moon. The color denotes the varying intensity of the image. Adapted with permission from [57].

diffusion.[56] From the rotational diffusion, a more comprehensive understanding can be obtained in many complex environments where translational and rotational diffusion are not simply proportional to one another, such as glassy materials. Indeed, when Janus particles with high enough optical contrast are viewed and magnified in an appropriate microscope, their images mimic the moon in all its phases (see Fig. 8). This enables the simultaneous tracking, at the single-particle level, of two rotational degrees of freedom.[56] Special tracking techniques have been developed to measure the orientation of two axes of a MOON particle from a single image, so that rotational dynamics can be acquired from a series of video frames. Also, the location of the center of MOON particles can be determined with modification of conventional tracking programs to give information about center-of-mass diffusion. In some cases,[56] the translational and rotational dynamics are largely coupled as they basically convey the same rheological properties of the environment. They can, however, be decoupled in more complex systems, for example in the case of hopping of colloids on a patterned surface[57] or for asymmetric colloidal clusters.[58] This illustrates the richness of information that rotational diffusion of Janus probes can provide.

5.3 Janus Particles as Solid Surfactants

Janus particles can be applied as an emulsion stabilizing agent. It was de Gennes' original idea that Janus particles would adsorb at a liquid–liquid or liquid–air interface to form a monolayer, though it is true that homogeneous particles with proper surface chemistry will also adsorb.[59] However, when the particle size is less than 10 nm, the adsorption energy onto a liquid–liquid interface for homogeneous particles becomes comparable to the
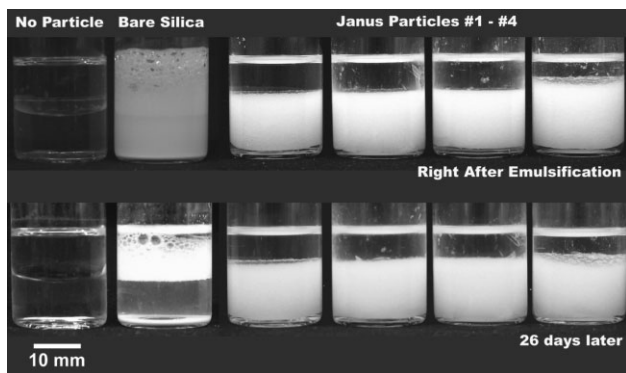
Figure 9. Photos of emulsions. Emulsification is carried out by the dispersing element running under 18 000 rpm for 1 min. Particles are 500 nm in diameter. The relative portion of hydrophobic and charged regions is parameterized by an angle α, the inclination angle corresponding to the radian from the center of hydrophobic part to its edge. Janus particle #1–#4 have geometries (α) of 45°, 47°, 57° and 72°, respectively. The emulsions stabilized by Janus particles can be dispersed in toluene, but not water, thereby indicating the emulsion type is water-in-oil.

Figure 10. Long-term stability of the emulsions described in Figure 9. Fraction of the resolved phase is plotted against time. The slight decrease may be due to the evaporation of the oil (toluene).

thermal energy, which implies that particles can be easily detached from the interface. On the other hand, Janus particles stabilize emulsions because they adsorb strongly at the liquid-liquid interface. Calculations show that Janus particles with proper surface chemistry improve the adsorption energy up to three times.[60] The consequences of varying the Janus balance have been explored in Reference [18].

We have investigated the ability of Janus amphiphilic particles to stabilize emulsions. Janus particles (1.0 wt%) were initially dispersed in toluene and then mixed with water. Emulsification was achieved using a Turux 18 dispersing element running at 18 000 rpm for 1 min. The emulsion was then held at room temperature and immediately photographed to record the position of the phase separation. Emulsion stability was evaluated by monitoring the changes of the phases. For all the emulsions stabilized by Janus particles studied, there were no obvious changes observed after 3 weeks. In a control experiment, the particles were harvested from the wax droplets before the silane vapor deposition. As demonstrated in Figure 9, particles without chemical modification cannot stabilize these emulsions. This also indicates that surfactant added during the synthesis has been cleaned in the washing step. Figure 10 shows tracking of the phase change over more than 3 weeks. The slight decrease in toluene and emulsion phase may be due to a small amount of evaporation. Hence, it is clear that Janus amphiphilic particles can stabilize water–toluene emulsions. For all the particles investigated with different Janus balance, water in toluene emulsions were formed and stabilized for extended times.

6. Conclusions and Outlook

The recent developments in Janus particle research described in this Progress Report now provide access to Janus particles with different surface chemistry and geometry. Moreover, new fabr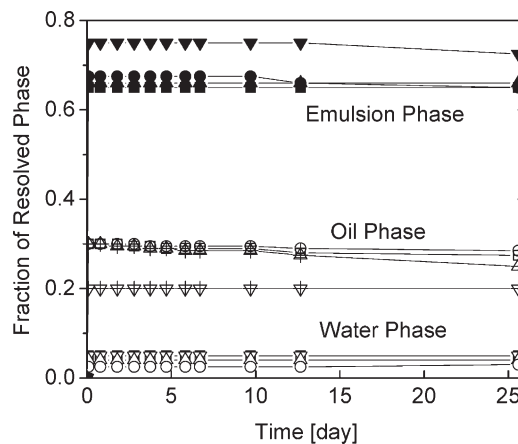ication methods have been formulated that give desirable control over not only surface chemical composition, but also the capacity to produce large quantities of monodisperse Janus particles. Looking to the future, we note the applications discussed above, some of which are already realized, some of which need further development. The research in self-assembly already shows that intriguing hierarchical structures can be assembled by Janus particles, which do not form spontaneously when homogeneous particles are mixed. Fundamental research of this kind will continue to elucidate our understanding of the principles of the self-assembly process. Many aspects of future work will surely revolve around the malleability and environmental responsiveness of these structures, an aspect that to date in our opinion has seen too little attention.

As concerns theory and simulation on these systems, a key point is that although attractive energies are sufficiently strong to form stable structures, the experiments show dynamic rearrangement implying that the energies of attraction do not exceed a few $k_B T$, which in turn implies that the observed structures are likely to be equilibrated. This is exciting because the alternative scenario, structures that would be trapped in nonequilibrium history-dependent states, would be easy to imagine in the event of stronger attractive energies. To model such behavior, it is then reasonable to pursue equilibrium theory, and prospects are high for rapid progress. Many additional aspects of the statistical structure and spinodal phase behavior can be studied using the present simplest level of theory sketched in Section 3. These include the real-space pair correlation functions, collective partial structure factors relevant to small- and wide-angle scattering experiments, and the consequences of changing Janus balance, core diameter, and the range and functional form of the interparticle potentials. Moreover, recent theoretical and simulation studies of block copolymer solutions[61] suggest that the microphase spinodals at low particle volume fractions may be a useful indicator of the formation of clusters or aggregates, as experimentally observed for Janus colloids.[28,42] The theory can also be straightforwardly applied to Janus rod or discotic colloids. Furthermore, the Monte Carlo computer simulations performed to date by ourselves[28,42] and other groups in this field[51] demonstrate the potential for rapid advance of fundamental

understanding. At the time that these words are written, a special challenge is for experimentalists to match the progress already achieved by computer simulation. To this end, it will be necessary to find synthetic pathways in the laboratory to implement the multivalent structures that have been proposed in large quantities and in monodisperse form.

Acknowledgements

[1] P. G. de Gennes, *Rev. Mod. Phys.* **1992**, *64*, 645.
[2] J. N. Israelachvili, *Intermolecular and Surface Forces*, Academic Press, **1992**.
[3] J. R. Savage, D. W. Blair, A. J. Levine, R. A. Guyer, A. D. Dinsmore, *Science* **2006**, *314*, 795.
[4] P. Schall, I. Cohen, D. A. Weitz, F. Spaepen, *Science* **2004**, *305*, 1944.
[5] C. Casagrande, P. Fabre, E. Raphaël, M. Veyssié, *Europhys. Lett.* **1989**, *9*, 251.
[6] D. Dendukuri, T. A. Hatton, P. S. Doyle, *Langmuir* **2007**, *23*, 4669.
[7] Z. H. Nie, W. Li, M. Seo, S. Q. Xu, E. Kumacheva, *J. Am. Chem. Soc.* **2006**, *128*, 9408.
[8] T. Nisisako, T. Torii, T. Takahashi, Y. Takizawa, *Adv. Mater.* **2006**, *18*, 1152.
[9] A. Perro, S. Reculusa, S. Ravaine, E. B. Bourgeat-Lami, E. Duguet, *J. Mater. Chem.* **2005**, *15*, 3745.
[10] K. H. Roh, D. C. Martin, J. Lahann, *Nat. Mater.* **2005**, *4*, 759.
[11] H. Takei, N. Shimizu, *Langmuir* **1997**, *13*, 1865.
[12] O. Cayre, V. N. Paunov, O. D. Velev, *J. Mater. Chem.* **2003**, *13*, 2445.
[13] O. Cayre, V. N. Paunov, O. D. Velev, *Chem. Commun.* **2003**, 2296.
[14] V. N. Paunov, O. J. Cayre, *Adv. Mater.* **2004**, *16*, 788.
[15] K. Fujimoto, K. Nakahama, M. Shidara, H. Kawaguchi, *Langmuir* **1999**, *15*, 4630.
[16] Y. K. Takahara, S. Ikeda, S. Ishino, K. Tachi, K. Ikeue, T. Sakata, T. Hasegawa, H. Mori, M. Matsumura, B. Ohtani, *J. Am. Chem. Soc.* **2005**, *127*, 6271.
[17] W. C. Griffin, *J. Soc. Cosmet. Chem.* **1950**, *1*, 311.
[18] S. Jiang, S. Granick, *J. Chem. Phys.* **2007**, *127*, 161102.
[19] L. Hong, S. Jiang, S. Granick, *Langmuir* **2006**, *22*, 9495.
[20] R. Aveyard, B. P. Binks, J. H. Clint, *Adv. Colloid Interface Sci.* **2003**, *100*, 503.
[21] S. Jiang, S. Granick, *Langmuir* **2008**, *24*, 2438.
[22] S. Jiang, M. J. Schultz, Q. Chen, J. S. Moore, S. Granick, *Langmuir* **2008**, *24*, 10073.
[23] D. Andelman, R. E. Rosensweig, *J. Phys. Chem. B* **2009**, *113*, 3785.
[24] F. S. Bates, G. H. Fredrickson, *Phys. Today* **1999**, *52*, 32.
[25] G. H. Fredrickson, *The Equilibrium Theory of Inhomogeneous Polymers*, Oxford University, Oxford, UK **2005**.
[26] L. Leibler, *Macromolecules* **1980**, *13*, 1602.
[27] R. P. Sear, W. M. Gelbart, *J. Chem. Phys.* **1999**, *110*, 4582.
[28] L. Hong, A. Cacciuto, E. Luijten, S. Granick, *Langmuir* **2008**, *24*, 621.
[29] D. Chandler, in: *Studies in Statistical Mechanics*, Vol. 8 (Eds: E. W. Montroll, J. Lebowitz), Amsterdam, North Holland **1982**, 275.
[30] K. S. Schweizer, J. G. Curro, *Adv. Chem. Phys.* **1997**, *98*, 1.
[31] J. B. Hooper, K. S. Schweizer, *Macromolecules* **2005**, *38*, 8858.
[32] A. Jayaraman, K. S. Schweizer, *Macromolecules* **2008**, *41*, 9430.
[33] A. Jayaraman, K. S. Schweizer, *Langmuir* **2008**, *24*, 11119.
[34] L. M. Hall, K. S. Schweizer, *J. Chem. Phys.* **2008**, *128*, 234901.
[35] D. W. Oxtoby, *Annu. Rev. Mater. Res.* **2002**, *32*, 39.
[36] R. P. Sear, *J. Phys.: Condens. Matter* **2007**, *19*, 033101.
[37] J. A. Lewis, J. E. Smay, J. Stuecker, J. Cesarano, *J. Am. Ceram. Soc.* **2006**, *89*, 3599.
[38] A. Van Blaaderen, *Science* **2003**, *301*, 470.
[39] H. Onoe, K. Matsumoto, I. Shimoyama, *Small* **2007**, *3*, 1383.
[40] A. Terfort, N. Bowden, G. M. Whitesides, *Nature* **1997**, *386*, 162.
[41] S. C. Glotzer, M. J. Solomon, *Nat. Mater.* **2007**, *6*, 557.
[42] L. Hong, A. Cacciuto, E. Luijten, S. Granick, *Nano Lett.* **2006**, *6*, 2510.
[43] R. H. Hardin, N. J. A. Sloane, W. D. Smith, Tables of Spherical Codes with Icosahedral Symmetry http://www.research.att.com/~njas/icosahedral.-codes/.
[44] M. Klokkenburg, R. P. A. Dullens, W. K. Kegel, B. H. Erne, A. P. Philipse, *Phys. Rev. Lett.* **2006**, *96*, 037203.
[45] K. Van Workum, J. F. Douglas, *Phys. Rev. E* **2006**, *73*, 031502.
[46] V. N. Manoharan, M. T. Elsesser, D. J. Pine, *Science* **2003**, *301*, 483.
[47] C. De Michele, S. Gabrielli, P. Tartaglia, F. Sciortino, *J. Phys. Chem. B* **2006**, *110*, 8064.
[48] D. J. Wales, *Int. J. Mod. Phys. B* **2005**, *19*, 2877.
[49] D. J. Wales, J. P. K. Doye, M. A. Miller, P. N. Mortenson, T. R. Walsh, *Adv. Chem. Phys.* **2000**, *115*, 1.
[50] D. Zerrouki, B. Rotenberg, S. Abramson, J. Baudry, C. Goubault, F. Leal-Calderon, D. J. Pine, M. Bibette, *Langmuir* **2006**, *22*, 57.
[51] Z. L. Zhang, S. C. Glotzer, *Nano Lett.* **2004**, *4*, 1407.
[52] A. Stradner, H. Sedgwick, F. Cardinaux, W. C. K. Poon, S. U. Egelhaaf, P. Schurtenberger, *Nature* **2004**, *432*, 492.
[53] B. M. Discher, Y. Y. Won, D. S. Ege, J. C. M. Lee, F. S. Bates, D. E. Discher, D. A. Hammer, *Science* **1999**, *284*, 1143.
[54] S. Gangwal, O. J. Cayre, M. Z. Bazant, O. D. Velev, *Phys. Rev. Lett.* **2008**, *100*, 058302.
[55] J. R. Howse, R. A. Jones, A. J. Ryan, T. Gough, R. Vafabakhsh, R. Golestanian, *Phys. Rev. Lett.* **2007**, *99*, 048102.
[56] S. M. Anthony, L. Hong, M. Kim, S. Granick, *Langmuir* **2006**, *22*, 9812.
[57] M. Kim, S. A. Anthony, S. Granick, *Phys. Rev. Lett.* **2009**, *102*, 178303.
[58] M. Kim, S. A. Anthony, S. Granick, *Soft Matter* **2009**, *5*, 81.
[59] B. P. Binks, *Phys. Chem. Chem. Phys.* **2007**, *9*, 6298.
[60] B. P. Binks, P. D. I. Fletcher, *Langmuir* **2001**, *17*, 4708.
[61] B. Capone, C. Pierleoni, J.-P. Hansen, V. Krakoviack, *J. Phys. Chem. B* **2009**, *113*, 3629.